

Plasmon Excitations by Photoelectron Emission from Rare Gas Nanobubbles in Aluminum

R. S. Dhaka and S. R. Barman*

UGC-DAE Consortium for Scientific Research, Khandwa Road, Indore, 452001, Madhya Pradesh, India

(Received 28 July 2009; published 21 January 2010)

Aluminum bulk, surface, and multiple plasmons have been observed in the core-level spectra of rare gas (Ne, Ar, and Xe) nanobubbles in Al, whose intensities are even higher than those of Al metal. Both intrinsic and extrinsic bulk plasmons are detected, but they exhibit diametrically opposite intensity variation due to change in the size and implantation depth of the bubbles. Furthermore, the existence of bubble surface plasmon is demonstrated.

DOI: 10.1103/PhysRevLett.104.036803

PACS numbers: 73.20.Mf, 62.23.Pq, 73.21.-b, 79.60.-i

The study of plasmons in nanosystems has assumed immense importance in recent years for their potential application in subwavelength optics, data storage, microscopy and biosensors [1]. Rare gas (RG) bubbles in aluminum is an interesting embedded nanosystem, where the bubble radii have been reported to vary from fraction of a nm to less than 10 nm, depending on implantation conditions [2–7]. The repulsive pseudopotential of RG atoms in Al makes bubble formation energetically favorable [8]. Because of their small size and proximity to the Al surface, these bubbles exhibit quantum confinement and interference [9]. Dynamical screening of the RG core-hole by Al conduction electrons has been reported by x-ray photoelectron spectroscopy (XPS) [10–12]. The RG bubbles are overpressurized and thus can exist in liquid or solid state even at room temperature [2–7].

Study of collective plasmon modes on metal surfaces by XPS has been a subject of extensive research spanning several decades [13–25]. In particular, the intrinsic plasmon, which originates due to the positive potential of the hole in the photoemission final state, has attracted much attention. While studies on plasmon excitations so far have dealt with metal surfaces, adlayers, and nanosystems [1,13–26], no work exists on RG nanobubbles in Al. This is an interesting system because during photoemission the bubbles would act like embedded emitters of electrons that are partially isolated from the Al conduction electrons. Unlike atomic implants [27], the extent of this isolation can be varied by changing the bubble size. In fact, we have shown that due to the change in Al conduction electron screening, the RG core-level binding energy increases with the bubble size [10–12]. In this Letter, we report plasmon excitations by photoemission from implanted RG nanobubbles of varying size and depth. The importance of using photoemission to study the plasmons lies in the intrinsic plasmons that are not excited in electron energy loss spectroscopy (EELS) [2,3].

The RG bubbles were formed by bombarding ions of different implantation energies (E_i) on an atomically clean Al(111) surface held at 350 K [10–12]. XPS was per-

formed using an electron energy analyzer from Specs GmbH at a base pressure of 4×10^{-11} mbar. An energy resolution of 0.8 eV was used, which is suitable for the present purpose since the plasmon widths are 4–5 eV. Thus, higher count rate essential to record the weak plasmon signals (the concentration of RG atoms being $\leq 4\%$ [11,12]) was obtained. Asymmetric Lorentzians with Γ_R and Γ_L as right and left half widths, respectively [19,20], were used to simulate the plasmon line shapes, while Doniach-Šunjić line shape [28] was used for the main peak [16]. Plasmons corresponding to each component of the RG core-level peaks were considered separately. However, their widths were constrained to be equal.

A remarkable observation in Fig. 1 is that the plasmon loss peaks appear at same energies in all the RG core-level spectra, as depicted by the vertical lines. For example, the first and second loss peaks are at 10.4 and 15.4 eV. These correspond to the Al surface plasmon ($1\omega_s$) and bulk plasmon ($1\omega_p$) energies [16], respectively (bottom spectrum). Similarly, the peaks at 25.5 and 31 eV are exactly where Al related $1\omega_p + 1\omega_s$ and $2\omega_p$ multiple plasmons appear. From the areas of their deconvoluted line shapes (Fig. 1), the intensity ratios of $2\omega_p$ and $1\omega_p$ are 0.45 and 0.35 for Ar and Xe, respectively, which are similar to Al (0.46). Also, the $1\omega_s$ to $1\omega_p$ intensity ratio for Ar, Xe and Al are in good agreement, having values 0.7, 0.65, 0.65, respectively. Thus, based on similarity of energy positions and relative intensities, it is established that the loss peaks in the RG spectra are actually Al plasmons excited by photoemission from the nanobubbles.

We have shown in our earlier work that the implantation depth (d), the bubble radius (R), and the concentration of the RG atoms increase with E_i [10–12]. After implantation, the RG atoms undergo diffusion and for small E_i (concentration and d) the probability is high that they reach the surface and desorb out rather than coalesce to form bubbles. Hence, for small E_i , R is small. On the other hand, for larger E_i , the probability to form bigger bubbles increases. It was shown that $R \propto E_i^n$, with $n = 0.27, 0.5$, and 0.32 for Ne, Ar, and Xe, respectively [10–12].

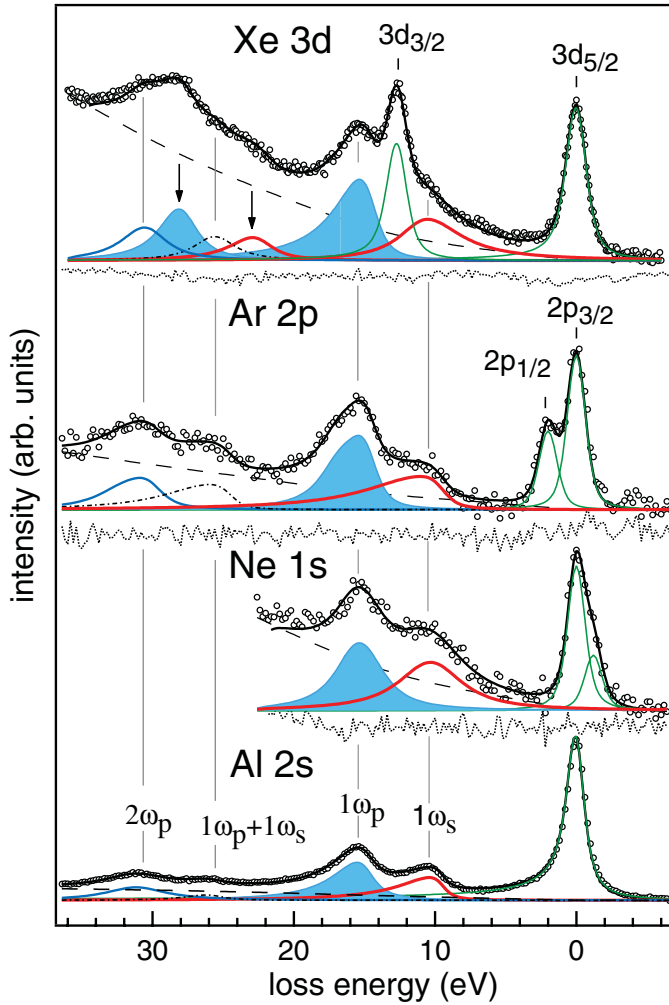


FIG. 1 (color). Ne $1s$, Ar $2p$, and Xe $3d$ core-level spectra of RG nanobubbles in Al (open circles) compared to the $2s$ spectrum of aluminum metal. The fitted curve (black line), the main peak components (green lines), the bulk plasmons: $1\omega_p$ (blue shading) and $2\omega_p$ (blue line), surface plasmon: $1\omega_s$ (red thick line), multiple plasmon: $1\omega_p + 1\omega_s$ (black dot dashes) and the inelastic Tougaard [32] background (black long dashes) are shown. The arrows show $1\omega_p$ and $1\omega_s$ related to Xe $3d_{3/2}$. The core-level main peaks have been normalized to the same height and aligned to zero loss energy. The residuals (short dashes) show the good quality of the fit.

In order to investigate the intrinsic and extrinsic processes in the Al related bulk plasmon, we study its behavior with E_i . In Fig. 2(a), a large increase in $1\omega_p$ intensity is observed between the spectra with $E_i = 0.3$ and 5 keV. The $1\omega_p + 1\omega_s$ and $2\omega_p$ intensities are also higher at 5 keV. However, between $E_i = 0.3$ and 1 keV spectra, $1\omega_p$ intensity is less in the latter [Fig. 2(a)]. The coupling parameter b for the $1\omega_p$ excitation is defined as its intensity divided by the RG main peak intensity, averaged over different measurements. As E_i decreases from 5 keV, for both Ne and Ar, b decreases until about the minimum at $E_i = E_{i:b_{\min}}$ [arrows in Figs. 2(b) and 2(c)]. Below $E_{i:b_{\min}}$, a clear

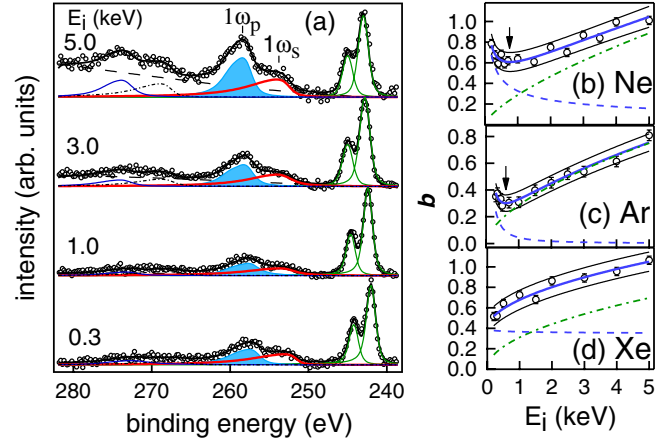


FIG. 2 (color online). (a) Ar $2p$ core-level spectra (open circles) as a function of implantation energy (E_i). The line-types have same meaning as in Fig. 1. b values for Ne $1s$ (b), Ar $2p$ (c), and Xe $3d$ (d) core-levels with the fitted curve (thick blue line), 90% prediction bands (black thin lines), b_i (blue dashes) and b_e (green dot-dashes) components.

upturn is observed for both Ne and Ar. Curiously, no such upturn is observed for Xe [Fig. 2(d)].

To explain the above unexpected variation of b , we first consider the extrinsic contribution (b_e) to $1\omega_p$. If photoemission occurs at an average depth of d , b_e is proportional to the path length ($d/\sin\theta$) that the electron traverses to reach the Al surface. Here, θ is the photoelectron emission angle and since the specimen orientation is kept unchanged during the measurement, $b_e \propto d$. Calculation of $d(E_i)$ using transport of ions through matter (TRIM) code gives $d \propto E_i^k$, where $k = 0.7, 0.6,$ and 0.5 for Ne, Ar, and Xe, respectively, with d ranging from 15–120 Å [10–12]. Thus, we obtain $b_e = q_e E_i^k$, where q_e is a proportionality constant.

The other contribution to b could arise from the intrinsic plasmon (b_i). The intrinsic plasmons would be excited because, due to the small size of the bubbles, screening of the positive core-hole by the Al conduction electrons will occur. However, b_i would decrease as the screening becomes weaker with increase in R . The extra-atomic relaxation energy, which is a measure of the screening, is known to be inversely proportional to the radius of the implanted RG atoms [27]. Hence, we propose that $b_i \propto 1/R^m$, where m could be somewhat different from unity for the bubbles [10–12]. As discussed earlier, $R \propto E_i^p$ and, consequently, $b_i = q_i/E_i^m = q_i/E_i^p$, where q_i is a proportionality constant and $p = nm$. Thus, an expression for $b = b_e + b_i = q_e E_i^k + q_i/E_i^p$ is obtained.

Using this equation, we have fitted $b(E_i)$ by varying q_e , q_i , and p [Figs. 2(b)–2(d)]. The fitted curves nicely reproduce the upturn for Ne and Ar. The prediction bands show the region where the experimental data fall with 90% probability considering random errors. From the fitting, we find q_e , q_i , and p to be about 0.3 (0.3), 0.35 (0.05), and 0.45 (1.4) for Ne (Ar), respectively. Smaller q_i and

larger p in Ar results in faster decrease of b_i compared to Ne [Figs. 2(b) and 2(c)].

In Figs. 2(b) and 2(c), the extrinsic (b_e) and intrinsic (b_i) plasmon intensities exhibit diametrically opposite behavior. b_i decreases as E_i increases and for $E_i \leq E_{i:b_{\min}}$, it is larger than b_e . On contrary, b_e increases as E_i increases and for $E_i \geq E_{i:b_{\min}}$, b_e dominates over b_i . The increase in b_e with E_i can be related to the increase in d , while decrease in b_i is due to increase in R . Thus, the upturn in b below $E_{i:b_{\min}}$ is related to the contrasting variation of b_e and b_i with E_i . However, note that the upturn is absent in Xe [Fig. 2(d)]. For $E_i \leq E_{i:b_{\min}}$, the bubbles are very small, in the verge of being single atom implants [10]. Theoretically, it was shown that for single atom implants, the extra-atomic relaxation energy (that determines b_i) is smallest for Xe and largest for Ne [12,27]. This explains why Xe does not exhibit the upturn, while it is most prominent in Ne.

An interesting observation is that the plasmons in the RG core-level spectra are more intense compared to Al metal (Fig. 1). b for Ne, Ar, and Xe are 1, 0.8, and 1.1, respectively, at $E_i = 5$ keV [Figs. 2(b)–2(d)]. In contrast, b for Al is about 0.5 [16]. For Al metal, the photoemission signal emerges from the surface as well as from deeper below, and the total signal is an integration over depth. Hence, for Al, b is independent of depth [16,18,19]. On contrary, for RG bubbles b increases with d , since here photoemission occurs from a localized region. Thus, for $E_i > E_{i:b_{\min}}$, b for RG bubbles gradually increases to values much larger than that of Al. However, for $E_i \leq E_{i:b_{\min}}$, where d is of the order of Al mean free path (≈ 15 – 20 Å), b for RG bubbles and Al metal are comparable.

Turning to the Al related surface plasmon ($1\omega_s$) in Ar $2p$ spectra, we find that its intensity increases with E_i [Fig. 2(a)]. The coupling parameter s (defined as the $1\omega_s$ intensity divided by the main peak) shows that it increases for all the three rare gases [Figs. 3(a)–3(c)]. The extrinsic surface plasmon (s_e) is excited only when the RG photoelectron traverses or interacts with the Al surface and thus it would be independent of E_i i.e. $s_e = \alpha$. The intrinsic surface plasmon (s_i) intensity would decrease with d as $s_i = \gamma'/d^t$ that implies $s_i = \gamma/E_i^t$, where $t > 0$. A fit using $s_e + s_i = \alpha + \gamma/E_i^t$ naturally fails to simulate the increase of s_e with E_i and $\gamma \approx 0$ showing that s_i is negligibly small.

This puzzle could be resolved by considering plasmons excited at the bubble-Al interface, well known in literature as bubble surface plasmons (BSP) [29–31]. BSP l -pole frequencies are given by $\omega_p(l+1)/(2l+1)$ that vary between $1\omega_p$ ($l=0$) and $1\omega_s$ ($l=\infty$). A peak corresponding to the $l=1$ dipole mode has been observed by EELS and its intensity was found to increase with bubble size [2,3,5,12]. This is in agreement with a theoretical calculation that predicted a R^3 dependence of the $l=1$ mode intensity [29]. These studies thus show that BSP

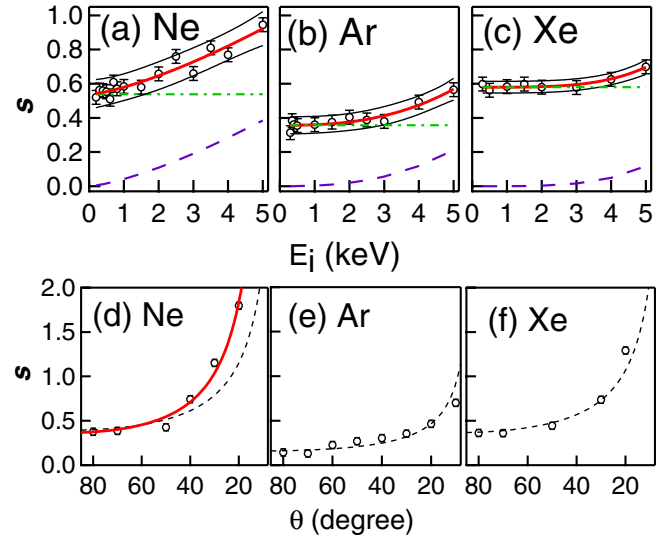


FIG. 3 (color online). s (open circle) as a function of E_i for (a) Ne $1s$, (b) Ar $2p$ and (c) Xe $3d$ core-levels with the fitted curve (thick red line), 90% prediction bands (black thin lines), and s_e (green dot-dashed line) and s_b (blue dashes) components. s as a function of emission angle (θ) for (d) Ne, (e) Ar, and (f) Xe for $E_i = 1.5$ keV.

intensity (s_b) increases with R , and this might explain the increase in s with E_i in Figs. 3(a)–3(c). To test this, we suggest $s_b = \beta E_i^j$, where β is a proportionality constant and j an exponent. s_b tends expectedly to zero in the limit of small E_i .

Using $s = s_e + s_b = \alpha + \beta E_i^j$ to simulate the experimental data, we obtain a good fit with $\alpha = 0.54, 0.36,$ and 0.58 , $\beta = 0.04, 0.003,$ and 0.0002 and $j = 1.4, 2.6,$ and 4 for Ne, Ar, and Xe, respectively. s_b is found to vary approximately as R^5 and turns out to be substantial for Ne and Ar: 40% and 35%, respectively, at $E_i = 5$ keV. For Xe, s_b is smallest (15%). Decrease in s_b can be explained by the decrease in R from Ne (15 Å, which is the weighted average of the bimodal R distribution) to Ar (9 Å), and Xe (6 Å) [11,12]. Possible reasons for the absence of identifiable BSP peak(s) in the spectra could be related to broadening due to contributions from all momenta observed in photoemission loss peaks [16,18,19]. Another possible reason of broadening could be the coupling of the BSP modes [30]. The interbubble distance a in Å [R/a] (bubble number density per c.c.) is 53 [0.28] (1.3×10^{19}), 26 [0.35] (1.1×10^{20}), and 12 [0.5] (11.3×10^{20}) for Ne, Ar, and Xe, respectively, at 5 keV. R/a can be used to assess the coupling, and the RG values are higher than Ni ($R/a = 0.15$), where coupling has been observed [30].

Angle dependent XPS measurements show that s for Ar and Xe increases substantially toward grazing emission ($\theta = 10$ – 20°) [Figs. 3(e) and 3(f)]. However, at $E_i = 1.5$ keV, s_b is negligible for both Ar and Xe [Figs. 3(b) and 3(c)], implying that s_e is solely responsible for the angular variation. For Al surface plasmon in O $1s$ spectra

from a monolayer of oxygen adsorbed on Al, s_e was found to exhibit a $u/\sin\theta$ dependence due to the proximity of photoelectrons to the Al surface as θ decreases, u being an adjustable parameter [22]. The same expression was used to describe $s_e(\theta)$ for Al metal [16]. To check its validity for bubbles and any deviation toward grazing angles, the fitting was done using lower weightage in nearly grazing angles. Still, good quality fit is obtained over the whole θ range with $u = 0.16$ and 0.37 for Ar and Xe [dashed lines in Figs. 3(e) and 3(f)].

In contrast, s for Ne is much larger (1.8 at 20°) compared to Ar (0.5) and Xe (1.3) and shows systematic deviation from the $u/\sin\theta$ curve toward grazing emission [dashed line, Fig. 3(d)]. This clearly indicates presence of an additional mechanism besides s_e . Note that for Ne, s_b is substantial at 1.5 keV in contrast to Ar or Xe [Figs. 3(a)–3(c)]. The outgoing photoelectrons from the bubbles have path length larger than a at grazing angles (for example, $a = 53 \text{ \AA}$, while path length given by $d/\sin\theta$ is 100 \AA at 30° for $d = 50 \text{ \AA}$). Because of larger path length, during the transport from the bubble (where photoemission occurs) to the Al surface, the photoelectrons will have higher probability of exciting BSP on other bubbles that might exist close to their path. Probability of excitation of BSP's on a spherical void in a metal by incident electrons has been found to be sizable in small scattering angles [31]. An estimate of $s_b(\theta)$ is obtained from steeper angular dependence of s given by $(u/\sin\theta)^w$ where $w = 1.5$ [red thick line, Fig. 3(d)]. In contrast, when s_b is negligible (as in Ar or Xe), $w \approx 1$.

To conclude, here we report study of collective excitations related to photoelectron emission from embedded objects of variable size and depth in a metal host. The aluminum bulk ($1\omega_p$), surface ($1\omega_s$) and multiple plasmons ($2\omega_p$, $1\omega_p + 1\omega_s$) arising from intrinsic and extrinsic processes are observed in the core-levels of the rare gas nanobubbles implanted in Al. The intrinsic plasmon is excited because of the nanometer size of the bubbles, and its intensity decreases with increasing bubble size. The extrinsic plasmon contribution increases with implantation depth. The variation of surface plasmon intensity with bubble size and emission angle unambiguously establishes the existence of the bubble surface plasmon that is most intense in Ne. The generality of the present work is established by studying three rare gases; however, interesting differences in their behavior are also observed. We envisage that this study will stimulate significant theoretical and experimental research on embedded nanosystems.

C. Biswas, A. K. Shukla, A. Chakrabarti, G. Amarendra, A. Gupta, P. Chaddah, and K. Horn are thanked for useful discussions and support. Max-Planck-Gesellschaft, Germany and Department of Science and Technology, Government of India are acknowledged for funding.

*barmansr@gmail.com

- [1] W.L. Barnes, A. Dereux, and T.W. Ebbesen, *Nature* (London) **424**, 824 (2003); J. Nelayah *et al.*, *Nature Phys.* **3**, 348 (2007).
- [2] R. Manzke, G. Crecelius, and J. Fink, *Phys. Rev. Lett.* **51**, 1095 (1983).
- [3] A. vom Felde *et al.*, *Phys. Rev. Lett.* **53**, 922 (1984).
- [4] S.E. Donnelly and C.J. Rossouw, *Science* **230**, 1272 (1985); C.J. Rossouw and S.E. Donnelly, *Phys. Rev. Lett.* **55**, 2960 (1985).
- [5] J. Fink, *Adv. Electron. Electron Phys.* **75**, 121 (1989).
- [6] S.E. Donnelly *et al.*, *Science* **296**, 507 (2002).
- [7] R.S. Dhaka *et al.*, *J. Appl. Phys.* **105**, 054304 (2009).
- [8] J.E. Inglesfield and J.B. Pendry, *Philos. Mag.* **34**, 205 (1976).
- [9] M. Schmid, W. Hebenstreit, P. Varga, and S. Crampin, *Phys. Rev. Lett.* **76**, 2298 (1996).
- [10] C. Biswas, A.K. Shukla, S. Banik, S.R. Barman, and A. Chakrabarti, *Phys. Rev. Lett.* **92**, 115506 (2004).
- [11] R.S. Dhaka and S.R. Barman, *Phys. Rev. B* **79**, 125409 (2009).
- [12] R.S. Dhaka *et al.*, *Phys. Rev. B* **77**, 104119 (2008).
- [13] V. Despoja, M. Šunjić, and L. Marušić, *Phys. Rev. B* **77**, 035424 (2008).
- [14] F. Yubero and S. Tougaard, *Phys. Rev. B* **71**, 045414 (2005).
- [15] S.R. Barman, C. Biswas, and K. Horn, *Phys. Rev. B* **69**, 045413 (2004).
- [16] C. Biswas, A.K. Shukla, S. Banik, V.K. Ahire, and S.R. Barman, *Phys. Rev. B* **67**, 165416 (2003).
- [17] S.R. Barman, P. Häberle, and K. Horn, *Phys. Rev. B* **58**, R4285 (1998).
- [18] S.M. Bose, S. Prutzer, and P. Longe, *Phys. Rev. B* **27**, 5992 (1983).
- [19] J.E. Inglesfield, *J. Phys. C* **16**, 403 (1983).
- [20] P.M.T. van Attekum and J.M. Trooster, *Phys. Rev. B* **18**, 3872 (1978).
- [21] P. Steiner, H. Höchst, and S. Hüfner, *Z. Phys. B* **30**, 129 (1978).
- [22] A.M. Bradshaw, W. Domcke, and L.S. Cederbaum, *Phys. Rev. B* **16**, 1480 (1977).
- [23] D.R. Penn, *Phys. Rev. Lett.* **38**, 1429 (1977).
- [24] W.J. Pardee *et al.*, *Phys. Rev. B* **11**, 3614 (1975).
- [25] M. Šunjić and D. Šokčević, *Solid State Commun.* **15**, 165 (1974).
- [26] S.R. Barman *et al.*, *Phys. Rev. Lett.* **86**, 5108 (2001); *Phys. Rev. B* **57**, 6662 (1998); *Phys. Rev. B* **61**, 12721 (2000); *Phys. Rev. B* **64**, 195410 (2001).
- [27] B.J. Wacławski, J.W. Gadzuk, and J.F. Herbst, *Phys. Rev. Lett.* **41**, 583 (1978); R.E. Watson, J.F. Herbst, and J.W. Willkins, *Phys. Rev. B* **14**, 18 (1976); P.H. Citrin and D.R. Hamann, *Phys. Rev. B* **10**, 4948 (1974).
- [28] S. Doniach and M. Šunjić, *J. Phys. C* **3**, 285 (1970).
- [29] M. Natta, *Solid State Commun.* **7**, 823 (1969).
- [30] A.A. Lucas, *Phys. Rev. B* **7**, 3527 (1973).
- [31] J.C. Ashley and T.L. Ferrell, *Phys. Rev. B* **14**, 3277 (1976).
- [32] S. Tougaard, *Surf. Sci.* **216**, 343 (1989).